Article

Discovery Medicine 2024; 36(187): 1627–1640
https://doi.org/10.24976/Discov.Med.202436187.149

TNFAIP3 Overexpression Inhibits Diffuse Large B-Cell Lymphoma Progression by Promoting Autophagy through TLR4/MyD88/NF-κB Signaling Pathway

Fangying Ning[1,2], Huafang Wang[2], Zuyu Liang[2], Jianping Lan[1,2,*]

[1]Suzhou Medical College of Soochow University, 215006 Suzhou, Jiangsu, China
[2]Cancer Center, Department of Hematology, Zhejiang Provincial People's Hospital (Affiliated People's Hospital), Hangzhou Medical College, 310014 Hangzhou, Zhejiang, China
*Correspondence: lanjp@163.com (Jianping Lan)
Published: 20 August 2024

Background: Tumor necrosis factor alpha induced protein 3 (TNFAIP3) is reportedly to have significant implications for autophagy regulation in various cancers. The current study aimed to decipher the role and mechanism of TNFAIP3 in diffuse large B-cell lymphoma (DLBCL) by modulating autophagy.
Methods: Information pertaining to the differential expression and prognostic role of *TNFAIP3* in DLBCL was gleaned from the Gene Expression Omnibus (GEO) database. The *TNFAIP3* expression levels in human DLBCL cells were detected by quantitative real-time polymerase chain reaction (qRT-PCR) and Western blotting. Cell counting kit-8 (CCK-8) and colony formation assays were employed to determine cell proliferation. Transwell assay and flow cytometry were applied to detect cell migration and apoptosis, respectively. Immunofluorescence and transmission electron microscope were used for the assessment of cell autophagy. The levels of apoptotic markers (caspase-3, cleaved-caspase-3, Bcl-2 Associated X (Bax), and B cell lymphoma-2 (Bcl-2)), autophagy indicators (the ratio of microtubule-associated proteins 1A/1B light chain 3 II and I (LC3II/LC3I), Sequestosome (p62)), and pathway proteins (toll-like receptor 4 (TLR4), myeloid differentiation primary response 88 (MyD88), Transcription Factor NF-Kappa-B P65 Subunit (p65), and phosphorylated-p65 (p-p65)) were assessed via Western blotting. Immunohistochemistry was employed to detect Ki67 expression in tumor tissues.
Results: *TNFAIP3* expression in DLBCL samples was downregulated, correlating with poor prognosis. *TNFAIP3* expression was also downregulated in DLBCL cells. It was found that *TNFAIP3* impeded cell proliferation and migration, and enhanced apoptosis of OCI-LY3 cells. Intervention with autophagy inhibitor 3-methyladenine (3-MA) markedly reversed apoptosis of OCI-LY3 cells induced by *TNFAIP3*. Besides, *TNFAIP3* induced autophagy via modulating the TLR4/MyD88/nuclear factor kappa B (NF-κB) signaling pathway. *In vivo* experiments showed that *TNFAIP3* expression in DLBCL was downregulated, and upregulation of *TNFAIP3* could inhibit tumor growth.
Conclusion: *TNFAIP3* inhibits DLBCL progression by inducing TLR4/MyD88/NF-κB pathway-mediated autophagy.

Keywords: *TNFAIP3*; diffuse large B-cell lymphoma; autophagy; TLR4/MyD88/NF-κB

Introduction

Diffuse large B-cell lymphoma (DLBCL) is a malignant tumor of immune cells originating from lymph nodes and peripheral lymph nodes [1,2]. The combination of the standard therapy—rituximab—with chemotherapy agents, including cyclophosphamide, doxorubicin, prednisone, and vincristine (R-CHOP), extends the overall survival in patients suffering from DLBCL [3,4]. Nevertheless, 40% of patients fail to respond to the treatment or undergo relapse following the treatment [5]. Hence, it is of clinical significance to identify potential therapeutic targets for DLBCL, improve the prognosis of patients, and develop personalized treatment plans.

Tumor necrosis factor alpha induced protein 3 (TNFAIP3), also known as zinc finger protein A20, has been found to be an effective anti-inflammatory factor in fundamental studies [6]. Its anti-inflammatory effect is often mediated by the inhibition of tumor necrosis receptor, interleukin-1 (IL-1) receptor, toll-like receptor (TLR), nucleotide-binding and oligomerization domain (NOD) receptor, T cell receptor, B cell receptor, and CD40 downstream nuclear factor kappa B (NF-κB) signaling pathway transduction [7]. Recent studies have found abnormal expression of TNFAIP3 in B-cell lymphoma [8], colorectal cancer [9], liver cancer [10], breast cancer [11], gastric cancer [12], and other tumors, which is associated with tumor onset, progression, and prognosis. Similarly, it is aberrantly expressed in bladder cancer, and the expression level is

strongly linked with the pathological grade, tumor metastasis, and invasion. Importantly, the serum level of TNFAIP3 has been found to be downregulated in DLBCL patients [13]. However, the potential role of TNFAIP3 in DLBCL has not been clarified.

Autophagy refers to lysosome-mediated degradation of damaged organelles and macromolecules via [14]. Recent studies reveal that aside from modulating normal cell growth and development, autophagy is also implicated in the altered autophagic viability of tumor cells [15–17]. It has been found that TNFAIP3 has a regulatory role in autophagy [18,19]. For example, TNFAIP3 ameliorates the degeneration of inflammatory human nucleus pulposus cells and Parkinson's disease by promoting autophagy [20,21]. Furthermore, *TNFAIP3* is involved in the drug resistance mechanism in the context of colon cancer by influencing the level of autophagy [22]. Therefore, drugs that regulate autophagy have a promising application for tumor treatment. However, the effect and mechanism of *TNFAIP3*-regulated autophagy in DLBCL remains to be clarified.

The anti-inflammatory effect of *TNFAIP3* depends on the inhibition of TLR and NF-κB signaling pathway [7]. TLR proteins are a group of key receptors in the immune system, which can recognize pathogen-related molecular patterns as well as endogenous injury-related molecular patterns and initiate immune responses [23]. TLR has been identified as a major component of infectious diseases, innate immunity, inflammation, and inflammation-mediated tumorigenesis [24]. TLR4, the most widely studied TLR, is activated mainly by the recognition of lipopolysaccharide (LPS) in the outer membrane of Gram-negative bacteria [25]. Once TLR4 is activated, the MyD88 adaptor is recruited to the receptor, initiating downstream signaling and activating the NF-κB pathway [26]. Extensively found in tissues and cells, the TLR4/MyD88/NF-κB axis mediates inflammatory factor release and has important implications for the onset and development of diverse disorders [27]. Activation of the TLR signaling pathway can induce cancer proliferation, invasion, survival, and metastasis [24,28]. TNFAIP3 can regulate TLR4 and the NF-κB pathway [29]. Here, we investigated the mechanism underlying the TNFAIP3-mediated suppression of DLBCL development, through which autophagy is induced. In terms of functionality, the impacts of TNFAIP3 on human DLBCL cell viability, migration, and apoptosis, as well as the role of TNFAIP3 in tumor growth *in vivo*, were confirmed in this study. In terms of mechanism, whether the TLR4/MyD88/NF-κB pathway mediates the process of TNFAIP3-triggered autophagy in human DLBCL cells was verified. The aim of this research is to expand the knowledge of the possible molecular mechanisms related to human DLBCL development.

Materials and Methods

Cell Culture, Transfection, and Grouping

Two human DLBCL cell lines (OCI-LY7 and OCI-LY3) and a human peripheral blood B lymphocyte cell line (IM-9) were obtained from the Nanjing Cobioer Biosciences Co., Ltd. (CBP60559, CBP60265, CBP60276, Nanjing, China). The origin of the cell lines was verified using the approved DNA-based method. The names of these cell lines were checked against the database documenting cell lines mistakenly identified by the International Committee for Cell Line Accreditation (ICLAC). The identity of these cell lines was further ascertained using short tandem repeat (STR) profiling. This approach detected no cross-contaminations in any of the acquired cell lines. Moreover, to ensure the absence of contamination and affirm the purity and integrity, all cell lines were tested for mycoplasma contamination. OCI-LY7 and OCI-LY3 cells were cultured in Iscove' modified Eagle medium (IMEM) medium supplemented with 10% fetal bovine serum (FBS) and a 1% mixture of penicillin-streptomycin (GIBCO, batch number: C11875500BT, Thermo Scientific, Shanghai, China). Concurrently, IM-9 cells were cultivated in RPMI 1640 medium supplemented with 10% FBS and 1% penicillin-streptomycin. The cells were incubated at 37 °C with 5% CO_2, and the media was refreshed every 2–3 days. Upon reaching 80–90% confluence, the cells were subjected to a 48-hour transfection process with oe-*TNFAIP3* or negative control (NC) lentivirus, followed by a 24-hour incubation.

The cells were categorized into three groups, namely control, oe-NC, and oe-*TNFAIP3*.

Data Download and Pre-Processing

The expression level of *TNFAIP3* in DLBCL was analyzed *in silico* with data obtained from the established datasets. The DLBCL-related microarray expression profile dataset GSE43677 was acquired from the Gene Expression Omnibus (GEO) database (https://www.ncbi.nlm.nih.gov/geo/). The probes in the microarray expression matrix were annotated with gene names according to the "SOFT formatted family file(s)" on the GPL6244 platform. According to the sample information in the "Series Matrix File(s)", the dataset was divided into DLBCL (n = 12) and control (n = 30) groups. *t*-test was conducted to compare the differences in *TNFAIP3* expression between DLBCL and control groups. Besides, the GSE10846 and GSE32918 datasets were obtained from the GEO database, and data in the two datasets were combined to investigate the prognostic role of TNFAIP3 in DLBCL using Kaplan–Meier curves. R 4.2.2 software (version 4.2.2, R Foundation for Statistical Computing, Vienna, Austria) was employed for plotting the Kaplan–Meier curves.

Quantitative Real-Time Polymerase Chain Reaction (qRT-PCR)

Total RNA from the cultured cells and tissues (from the mouse in the following Xenograft Model) was isolated using TRIzol method (Invitrogen, batch number: 15596018, Carlsbad, CA, USA) and then reverse-transcribed using a commercial reverse transcription kit (Invitrogen, batch number: K1622, Carlsbad, CA, USA) to generate cDNA at 37 °C for 15 min and enzyme inactivation at 98 °C for 5 min. The reverse transcription-free (RTF) qRT-PCR system was configured by diluting 10 times and it was used as a template. In qRT-PCR, 10 µL mixture, 1 µL PCR forward primer (10 µM), 1 µL reverse primer (10 µM), 1 µL cDNA template, and 7 µL ddH_2O was added to each reaction containing SYBR premix EX TAQ II (TaKaRa, Dalian, China). The cDNA samples were subjected to PCR set with pre-determined thermal cycling conditions: activation (95 °C, 3 min), denaturation (95 °C, 12 s), and annealing (62 °C, 40 s), and repeated for 40 cycles. The $2^{-\Delta\Delta C(t)}$ method was employed to compute the relative gene expression. The corresponding primer sequences utilized in this experiment include: *TNFAIP3* (human): forward 5′-CTTGTGGCGCTGAAAACGAA-3′, reverse 5′-GCAGTTGGGCGTTTCACATT-3′; Glyceraldehyde-3-Phosphate Dehydrogenase (*GAPDH*) (human): forward 5′-GAAGGTCGGAGTCAACGGAT-3′, reverse 5′-CTTCCCGTTCTCAGCCATGT-3′; *TNFAIP3* (mice): forward 5′-CAGTTTTGCCCACAGTTCCG-3′, reverse 5′-CCACTGTCCTTCAGGGTCAC-3′; *GAPDH* (mouse): forward 5′-TGTGGGCATCAATGGATTTGG-3′, reverse 5′-ACACCATGTATTCCGGGTCAAT-3′.

Western Blotting

Total proteins were extracted from cells and tissues, followed by protein quantification using the BCA kit (Beyotime, batch number: P0010S, Shanghai, China). The isolated proteins were separated by means of SDS-PAGE system (Beyotime, batch number: P0015A, Shanghai, China). Following protein denaturation, each well on the SDS-PAGE gel (Beyotime, batch number: ST628, Shanghai, China) was added with 20 µg of protein. Then, the separated proteins were transferred to polyvinylidene fluoride (PVDF) membranes (Beyotime, batch number: FFP24, Shanghai, China), which were subsequently blocked with a 10% skim milk solution (Beyotime, batch number: P0216-300 g, Shanghai, China) for 2 h. The PVDF membranes were incubated with an array of primary antibodies at 4 °C overnight, including anti-Bcl-2 Associated X (Bax) (1:1000, ab32503, Abcam, Cambridge, UK), anti-B cell lymphoma-2 (Bcl-2) (1:1000, ab32124, Abcam, Cambridge, UK), anti-caspase-3 (1:5000, ab32351, Abcam, Cambridge, UK), anti- microtubule-associated proteins 1A/1B light chain 3 (LC3) (1:1000, 14600-1-AP, Wuhan Tianying, Wuhan, China), anti-p62 (1:5000, 18420-1-AP, Wuhan Tianying, Wuhan, China), anti-TNFAIP3 (1:500, 23456-1-AP, Wuhan Tianying, Wuhan, China), anti-TLR4 (1:500, 19811-1-AP, Wuhan Tianying, Wuhan, China), anti-MyD88 (1:1000, 23230-1-AP, Wuhan Tianying, Wuhan, China), anti-Transcription Factor NF-Kappa-B P65 Subunit (p65) (1:500, 10745-1-AP, Wuhan Tianying, Wuhan, China), anti-phosphorylated-p65 (p-p65) (1:1000, #3033, Cell Signaling Technology, Danvers, MA, USA), and anti-GAPDH (1:2000, ab63512, Abcam, Cambridge, UK). After washing with TBST (Beyotime, batch number: ST677-100 mL, Shanghai, China) three times, the membranes were incubated with goat anti-rabbit IgG H&L (HRP) (1:2000, ab6721, Abcam, Cambridge, UK) at room temperature for 2 h, followed by TBST washing for three times. The proteins were imaged with the help of Electronics Components Laboratory (ECL) chemiluminescent solution (Plile gene, batch number: P1000, Beijing, China) for color development. Band intensities were quantitatively analyzed utilizing the ImageJ software (version 1.48, National Institutes of Health, Bethesda, MD, USA). The relative protein expression was computed by determining the ratio of target protein gray value to GAPDH gray value.

Cell Counting Kit-8 (CCK-8) Assay

Stably transfected cells were harvested and centrifuged at 1000 rpm for 5 min. Then, the supernatant was discarded and the cell pellets were resuspended in fresh culture medium. Cell suspensions (100 µL/well) were inoculated in 96-well plates, and the plates were incubated at 37 °C with 5% CO_2 (Thermo Scientific, batch number: Heracell 150i, Shanghai, China) for 24 h. Each well was added with 10 µL CCK-8 kit (Beyotime, batch number: C0037, Shanghai, China). After incubation for 2 h, the absorbance was detected at 450 nm by a microplate reader (Wuxi Hiwell Diatek, batch number: DR-3518G, Wuxi, China).

Colony Formation Assay

The cultured cells (200 cells/well) were seeded into 6-well plates and incubated in a 5% CO_2 atmosphere at 37 °C for 14 days. After colonies were formed, the cells were subjected to gentle PBS washing twice. Subsequently, each well was fixed with 1 mL of anhydrous methanol (Sinopharm, batch number: 10009218, Beijing, China) for 15 min. After absorption of the methanol, the cells were stained with an appropriate amount of crystal violet (Beyotime, batch number: C0121, Shanghai, China) for 20 min. Excess crystal violet was then washed off with PBS. After air drying at room temperature, the 6-well plates were photographed.

Flow Cytometry

After 24 hours of cultivation, cells from each group were digested using 0.25% trypsin without Ethylene Diamine Tetraacetic Acid (EDTA). After terminating digestion, the cells were subjected to centrifugation at 1500 rpm

for 5 min. The cell pellets were then resuspended in pre-cooled PBS (Beyotime, batch number: C0221A, Shanghai, China) twice, each time coupled with a centrifugation procedure at 1500 rpm for 5 min. Afterward, 300 µL of binding buffer was added for cell resuspension, followed by the addition of annexin V-FITC (5 µL). After 15-min incubation at room temperature under light-protected conditions, propidium iodide (PI; 10 µL) staining was performed, and the cells were incubated at room temperature for another 10 min under light-protected conditions. Finally, the cells were examined by flow cytometry (Beckman, CytoFLEX S, Shanghai, China), and the data were analyzed using CELL Quest software (BD Biosciences).

Transwell Assay

Cells were harvested and digested using trypsin. Digestion was terminated using serum-free medium, followed by centrifugation. The cells were resuspended in serum-free medium and adjusted to a density of 1×10^5 cells/mL. Each well of the Transwell chamber was added with 200 µL of cell suspension. The lower chamber was filled with complete medium supplemented with 10% FBS, followed by 24-h incubation at 37 °C with 5% CO_2. Then, the Transwell chamber was carefully removed, with the medium within the chamber aspirated. The medium was discarded from the lower chamber, and the chamber was washed with PBS twice. The chambers were fixed with anhydrous methanol for 30 min, air-dried, and stained with crystal violet (Beyotime, batch number: C0121, Shanghai, China) for 20 min. After removal of the crystal violet solution, the chambers were subjected to PBS washing twice to eliminate excess stain. Non-migrating cells in the smaller chambers were gently cleared using a cotton swab. The cells were observed under a microscope (Leica, batch number: DM3000, Wetzlar, Germany) with 200× magnification. The microscopic observation was coupled with cell counting in three randomly chosen fields per group.

Immunofluorescence

In a sterile environment, cells at an appropriate density were seeded into a 12-well plate for cultivation. When a cell monolayer was formed in each well, the medium was removed, and the cell monolayer was subjected to PBS washing. Then, the cells were fixed at room temperature with 3% formaldehyde solution (Sinopharm, batch number: 10010018, Beijing, China) and permeabilized via 1% Triton X-100 (Solarbio, batch number: T8200, Beijing, China), followed by three washes with PBS. Next, an appropriate amount of 3% bovine serum albumin (BSA) blocking solution (Solarbio, batch number: SL038, Beijing, China) was added to each well, followed by a 30-min incubation at room temperature. Subsequently, each well was added with 50 µL of diluted LC3 primary antibody (1:250) and incubated at 4 °C overnight. The samples were then washed three times with PBS. FITC Goat Anti-Rabbit IgG (H+L) (ABclonal Technology, batch number: AS011, Shanghai, China) secondary antibody, mixed with DAPI (Beyotime, batch number: C1005, Shanghai, China), was diluted to a concentration of 1:500. Following incubation with this mixture at room temperature for 1 h, the samples were shielded from light and then subjected to PBS washing thrice. Finally, the slides were mounted and examined by means of laser confocal scanning microscopy (Perkin Elmer, Waltham, MA, USA).

Transmission Electron Microscope (TEM)

Cells were subjected to fixation with 2.5% glutaraldehyde, followed by washing with pre-cooled PBS thrice. Cells were subsequently dehydrated through gradient ethanol and acetone solutions. The cells were immersed in paraffin overnight at room temperature. Afterward, more paraffin was added, followed by solidification via heating in an oven. The paraffin cell block was then trimmed to generate sections, which were subjected to 20-min sodium acetate staining. Following staining, the sections were promptly washed thrice with double-distilled water. Excess water was removed by filter paper, and the slides were left to air-dry in a petri dish. Next, the grids were placed in another petri dish along with the slides for staining and cleaning with lead citrate. After drying, the samples were subjected to observation via transmission electron microscopy (JEM-1400 Flash, JEOL, Beijing China).

Construction of a Mouse Xenograft Model

BALB/c nude mice (4–5 weeks old, 15–20 g, n = 12) were acquired from Yangzhou University Animal Hospital (Yangzhou, China). After one week of acclimatization, the mice were randomly divided into two groups (n = 6). The mouse model was constructed according to the previous described methods [30]. When the mice reached the age of 6–7 weeks, 1×10^7 OCI-LY3 cells transfected with oe-NC- or oe-*TNFAIP3* were inoculated into the right axillary fossa of each animal via subcutaneous injection. Four weeks later, all nude mice were euthanized by carbon dioxide asphyxiation and Zoletil (0.5 mg/100 g). The tumor tissues were collected for further assays. This study was approved by the Institutional Animal Care and Use Committee of Yangzhou University (No: 202305011).

Tumor Weight and Volume

Tumor volume in each mouse was measured every 4 days for successive 4 weeks, with the dimensions required for calculation measured using vernier calipers. Tumor volume (V) was calculated using the formula in the following:

Tumor volume = 0.5 × a (the longest diameter) × b (the shortest vertical diameter) ^{2}.

Four weeks later, all nude mice were euthanized, and their tumors were photographed and weighed.

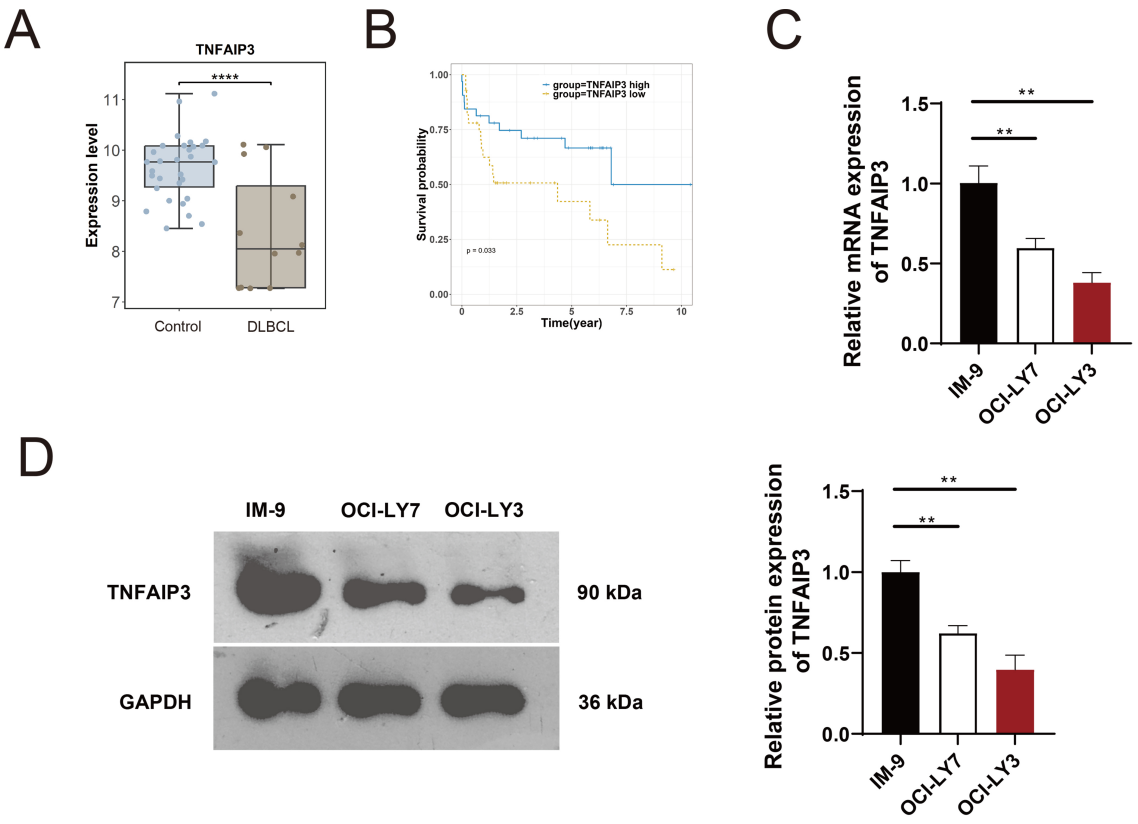

Fig. 1. Tumor necrosis factor alpha induced protein 3 (*TNFAIP3*) expression was downregulated in human diffuse large B-cell lymphoma (DLBCL) cells. (A) Bioinformatics analysis of *TNFAIP3* differential expression between DLBCL (N = 12) and control (N = 30) groups (GSE43677 dataset). (B) Kaplan–Meier survival curves of DLBCL patients manifesting different *TNFAIP3* expression levels (high and low; based on GSE10846 and GSE32918 datasets). (C) *TNFAIP3* mRNA expression levels in human DLBCL cell lines (OCI-LY7 and OCI-LY3) and human peripheral blood B lymphocyte cell line (IM-9) (n = 3). (D) Western blotting detection of TNFAIP3 protein and the quantification of its level in IM-9, OCI-LY7 and OCI-LY3 cells (n = 3). $^{**}p < 0.01$, $^{****}p < 0.0001$. GAPDH, Glyceraldehyde-3-Phosphate Dehydrogenase.

Immunohistochemistry

Paraffin-embedded xenograph tumor tissues were prepared and sectioned into slice with a thickness of 4 µm each. These sections were then routinely dewaxed using xylene (Sinopharm, batch number: 10023418, Beijing, China), followed by rehydration through a gradient series of alcohol. Endogenous peroxidase was blocked and inactivated by treating the sections with 3% H_2O_2 (Sinopharm, batch number: 10011208, Beijing, China) for 10 min. For antigen retrieval, the sections were heated in 0.01 mol/L sodium citrate buffer (pH 6.0; Beyotime, batch number: P0083, Shanghai, China) using a microwave oven for 15 min. The sections were then blocked with 5% BSA for 20 min. After an overnight incubation with anti-Ki67 antibody (Abcam, ab15580, Shanghai, China) at 4 °C , the sections were incubated with goat anti-rabbit secondary antibody (IgG Rabbit L (HRP), Abcam, ab6721, Shanghai, China) for 20 min. Following PBS washing, color development was carried out using DAB. Hematoxylin (Solarbio, batch number: G1080, Beijing, China) was used for counterstaining, after which the sections were dehydrated, cleared, and mounted using neutral gum. Finally, the sections were observed under a microscope (Leica, batch number: DM3000, Wetzlar, Germany).

Statistical Analysis

All data are expressed as mean ± standard deviation (SD). One-way analysis of variance (ANOVA) with Tukey's post-hoc test was used for comparing the differences among multiple groups, and *t*-test was employed for comparing the differences between two groups. GraphPad 7.0 software (GraphPad Software, San Diego, CA, USA) and R software (version 4.2.2, R Foundation for Statistical Computing, Vienna, Austria) were employed for statistical analyses and plot visualization, respectively. Differences between groups were considered statistically significant if $p < 0.05$.

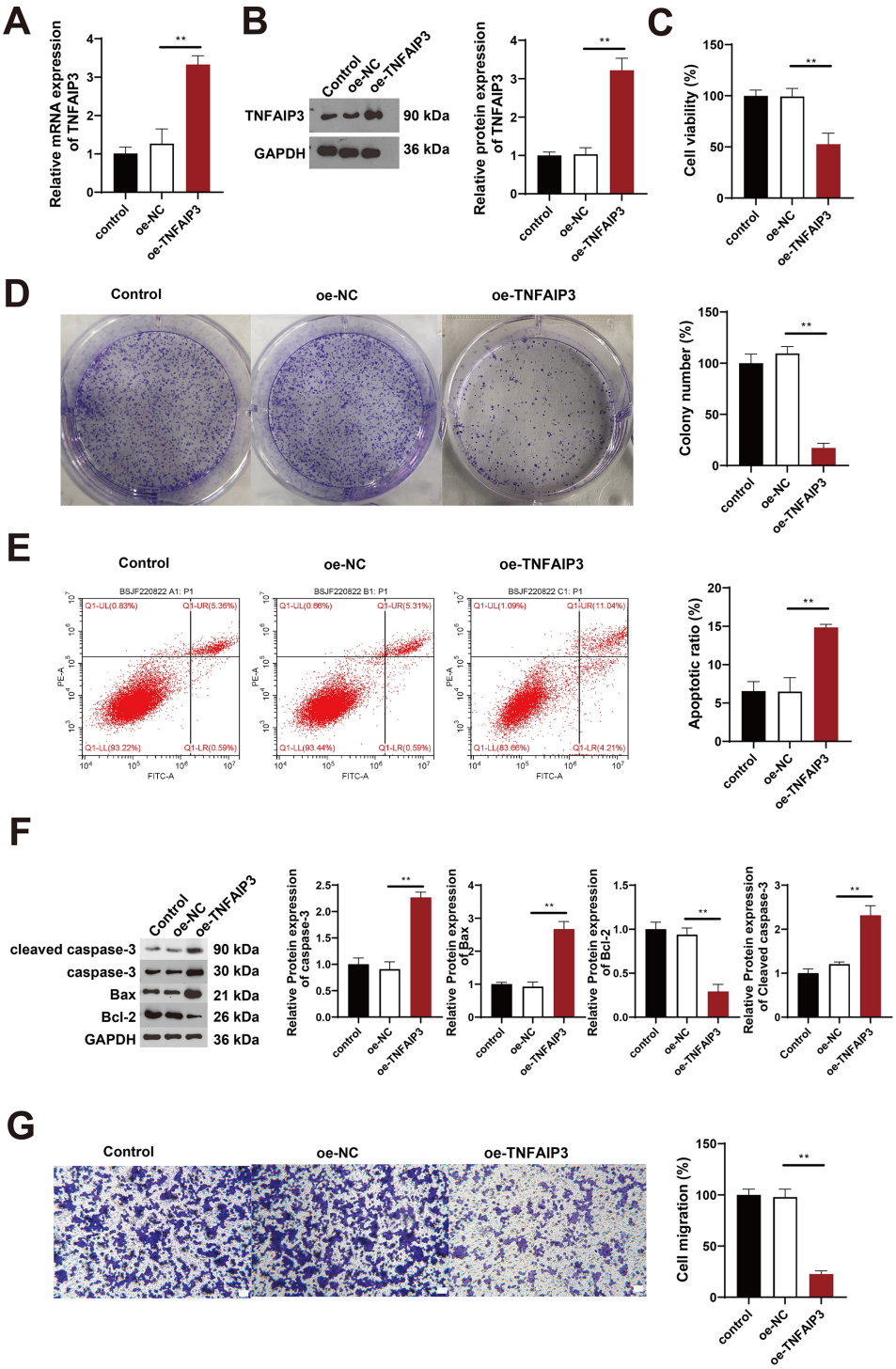

Fig. 2. *TNFAIP3* overexpression inhibited proliferation and migration of human DLBCL cells. Oe-negative control (NC) and oe-*TNFAIP3* overexpression lentiviral vectors were constructed and transfected into OCI-LY3 cells for 48 h, and the transfected cells were cultured for another 24 h. (A) *TNFAIP3* mRNA expression level in OCI-LY3 cells (n = 3). (B) Western blotting detection of TNFAIP3 protein and the quantification of its level in OCI-LY3 cells (n = 3). (C) OCI-LY3 cell viability as measured by cell counting kit-8 (CCK-8) assay (n = 3). (D) Colony formation assay photographs depicting proliferation of OCI-LY3 cells and the quantification of colony number in each group (n = 3). (E) Apoptosis levels of OCI-LY3 cells, as visualized by flow cytometry assay results (n = 3). (F) Western blotting detection of caspase-3, Bcl-2 Associated X (Bax), and B cell lymphoma-2 (Bcl-2) and the quantification of their protein levels in OCI-LY3 cells (n = 3). (G) Transwell assay photographs and the quantification of migrating OCI-LY3 cells (n = 3). Scale bar: 50 μm. $^{**}p < 0.01$.

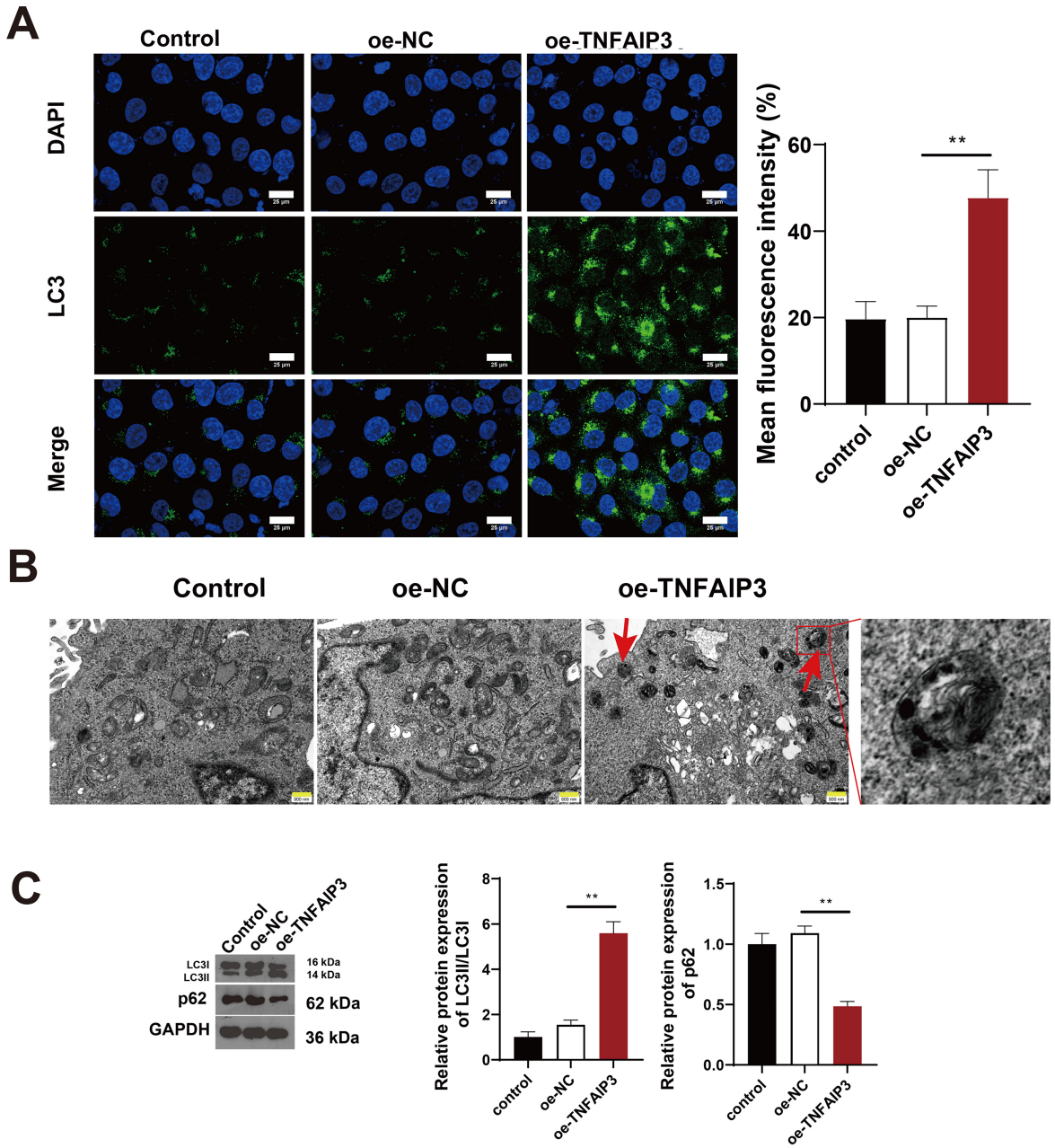

Fig. 3. *TNFAIP3* overexpression induced autophagy in human DLBCL cells. (A) Analysis of microtubule-associated proteins 1A/1B light chain 3 (LC3) expression in OCI-LY3 cells by fluorescent staining and the quantification of fluorescence intensity (n = 3). Scale bar: 25 µm. (B) Transmission electron microscope (TEM) observation of autophagosomes in the cells (n = 3). The red arrows denote autophagosomes. Scale bar: 500 nm. (C) Western blotting detection of LC3I, LC3II and p62, and the quantification of p62 protein level and LC3II/LC3I ratio in OCI-LY3 cells. $^{**}p < 0.01$.

Results

TNFAIP3 is Downregulated in DLBCL and Positively Correlated to DLBCL Prognosis

Bioinformatics analysis of genetic expression in DLBCL samples (based on the GSE43677 dataset), revealed that the *TNFAIP3* expression was downregulated in human DLBCL samples, relative to the control ($p < 0.001$, Fig. 1A). Furthermore, Kaplan–Meier curves showed that DLBCL patients in high *TNFAIP3* expression group had longer survival than those in low *TNFAIP3* expression group ($p = 0.033$, Fig. 1B). We also found that *TNFAIP3* expression was downregulated in human DLBCL cell lines, OCI-LY7 and OCI-LY3, compared to the expression level in human peripheral blood B lymphocyte cell line IM-9 ($p < 0.05$, Fig. 1C,D).

TNFAIP3 Overexpression Decreases the Proliferation and Migration of Human DLBCL Cells

OCI-LY3 cells with the lowest expression of *TNFAIP3* were selected for the subsequent functional experiments. OCI-LY3 cells were transfected with oe-NC and oe-*TNFAIP3* overexpression lentiviral vectors. Results showed that *TNFAIP3* was strongly upregulated in the oe-*TNFAIP3* group, versus the oe-NC group ($p < 0.01$, Fig. 2A,B). On the other hand, according to the results of CCK-8 and colony formation assays, OCI-LY3 cell proliferation decreased significantly after oe-*TNFAIP3* transfection ($p < 0.01$, Fig. 2C,D). Subsequently, flow cytometry analysis demonstrated that the oe-*TNFAIP3* group had a markedly higher proportion of apoptotic OCI-LY3 cells than the oe-NC group ($p < 0.01$, Fig. 2E). Similarly, the levels of the apoptotic proteins, caspase-3 and Bax were notably elevated in the oe-*TNFAIP3* group relative to the oe-NC group, while the Bcl-2 level was reduced ($p < 0.01$, Fig. 2F). Additionally, as corroborated via Transwell assay, the number of migrating OCI-LY3 cell was notably lowered following oe-*TNFAIP3* transfection ($p < 0.01$, Fig. 2G).

TNFAIP3 Overexpression Inhibits Malignant Phenotypes of Human DLBCL Cells by Promoting Autophagy

Abnormal regulation of autophagy emerges as a new pathological hallmark of human malignancy [31]. The current study assessed the effects of manipulating the expression of TNFAIP3, which regulates autophagy, on OCI-LY3 cell viability. LC3 is an indicator of the autophagic process, which mainly functions in autophagic vesicle generation [32]. Through fluorescent staining, LC3 was found to be localized in the cytoplasm and was markedly increased in the oe-*TNFAIP3* group, in comparison with the oe-NC group (Fig. 3A). Subsequently, autophagosomes in the cells were counted with the assistance of TEM, which showed a notable increase in autophagic vesicles in the oe-*TNFAIP3* group, relative to the oe-NC group (Fig. 3B). As confirmed via Western blotting, level of p62, which is a key regulator of autophagy [33], was remarkably downregulated, while levels of LC3II/LC3I, which can target autophagosomes to mitochondria and induce mitochondrial autophagy [34], were significantly upregulated, in the oe-*TNFAIP3* group, as compared to the oe-NC group ($p < 0.01$, Fig. 3C). To assess the impact of autophagy on OCI-LY3 cells, these cells were treated with autophagy inhibitor 3-methyladenine (3-MA) (2.5 mM), in addition to *TNFAIP3* overexpression. Results showed that 3-MA markedly elevated OCI-LY3 cell proliferation in comparison with the oe-*TNFAIP3* group ($p < 0.01$, Fig. 4A,B). Additionally, corroborated by flow cytometry, the apoptosis level of OCI-LY3 cells in the oe-*TNFAIP3* + 3-MA group was prominently attenuated, as compared to the oe-*TNFAIP3* group ($p < 0.05$, Fig. 4C). Besides, Transwell assay showed that 3-MA intervention prominently reversed the suppressive function of oe-*TNFAIP3* in OCI-LY3 cell migration ($p < 0.01$, Fig. 4D). Furthermore, immunofluorescence assay showed that LC3 content in the oe-*TNFAIP3* + 3-MA group was markedly lower than in the oe-*TNFAIP3* group (Fig. 4E). In the oe-*TNFAIP3* group, the p62 protein expression was significantly downregulated, while the LC3II/LC3I ratio became significantly higher ($p < 0.01$, Fig. 4F).

TNFAIP3 Overexpression Promotes Autophagy in Human DLBCL Cells by Blocking the TLR4/MyD88/NF-κB Axis

Next, whether *TNFAIP3* overexpression could induce autophagy through the TLR4/MyD88/NF-κB axis in human DLBCL cells was investigated. As confirmed via Western blotting, in comparison with the oe-NC group, the oe-*TNFAIP3* group exhibited substantially downregulated levels of TLR4, MyD88, and p-p65/p65 ($p < 0.01$, Fig. 5A). Subsequently, in addition to overexpressing *TNFAIP3*, OCI-LY3 cells were pre-treated with 20 ng/mL lipopolysaccharide (LPS), an agonist of TLR4. The TLR4, MyD88, and p-p65/p65 levels were substantially higher in the oe-*TNFAIP3* + LPS group than in the oe-*TNFAIP3* group ($p < 0.01$, Fig. 5B). CCK-8 assay results demonstrated that OCI-LY3 cell viability was dramatically increased in the oe-*TNFAIP3* + LPS group, versus the oe-*TNFAIP3* group ($p < 0.01$, Fig. 5C). In terms of autophagy proteins, LPS dramatically upregulated p62 level and downregulated LC3II/LC3I level in the oe-*TNFAIP3* + LPS group than in the oe-*TNFAIP3* group ($p < 0.05$, Fig. 5D).

TNFAIP3 Overexpression Suppresses DLBCL Tumor Growth in Vivo

The tumor suppressive effect of *TNFAIP3* was assessed *in vivo*. Firstly, changes in tumor volume were measured, and tumors were weighed. Results showed that the volume and size of tumor were smaller in the oe-*TNFAIP3* group than in the oe-NC group ($p < 0.05$, Fig. 6A,B). Subsequently, immunohistochemistry was performed to assess the Ki67 expression in the tumor tissues. We found that the Ki67 expression in the oe-*TNFAIP3* group was decreased, relative to the oe-NC group (Fig. 6C). On the other hand, as confirmed through qRT-PCR and Western blotting, *TNFAIP3* expression was elevated in the oe-*TNFAIP3* group in comparison with the oe-NC group ($p < 0.01$, Fig. 6D,E).

Discussion

DLBCL is a type of non-Hodgkin's lymphoma, characterized by the diffuse malignant proliferation of large B lymphocytes. This lymphoma exhibits considerable heterogeneity and invasiveness, accounting for a high incidence rate [35,36]. Although immunotherapy emerged as the new type of cancer treatment method for DLBCL in recent years, further research efforts are still warranted to explore poten-

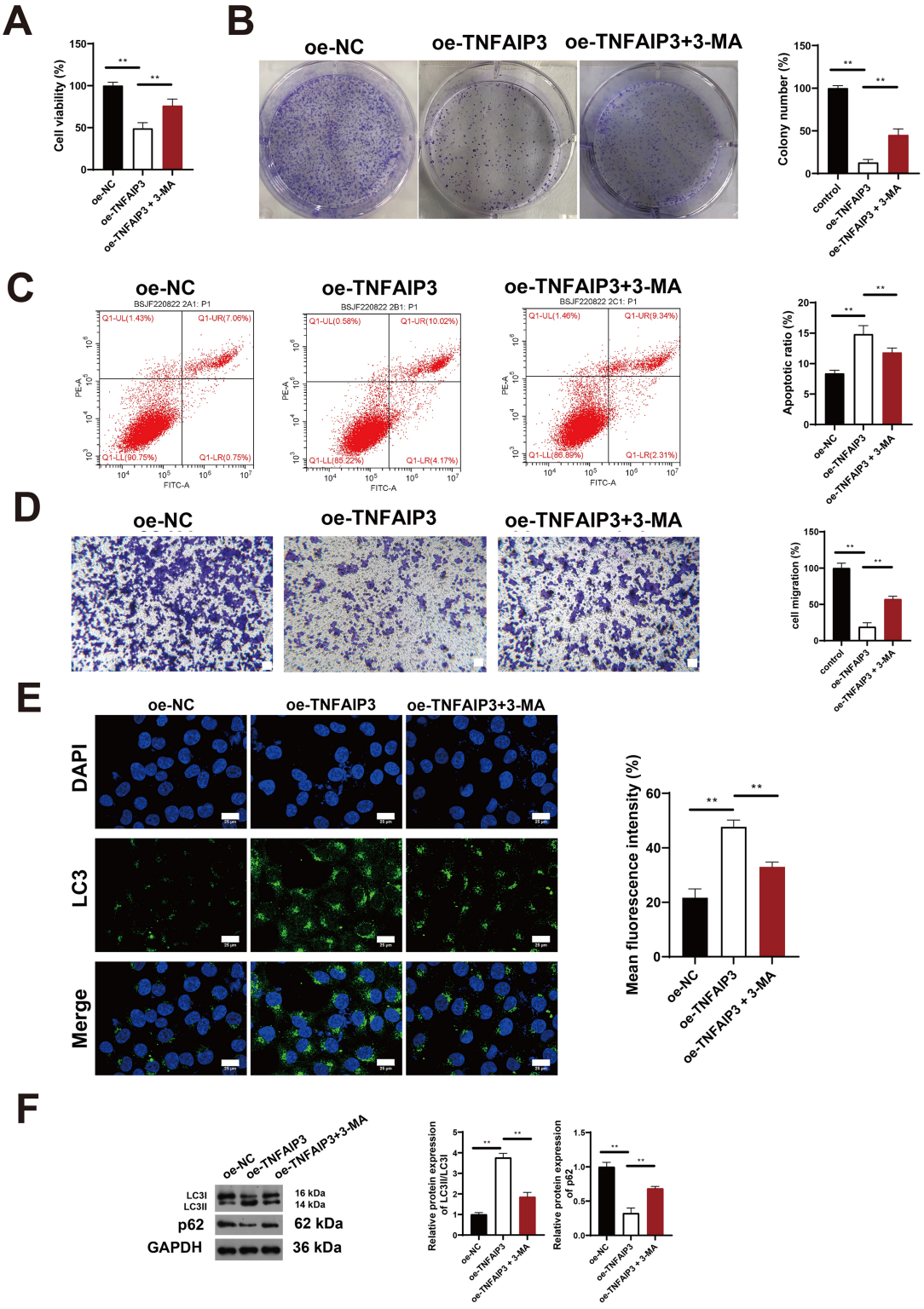

Fig. 4. *TNFAIP3* overexpression-induced autophagy inhibited proliferation and migration of human DLBCL cells. In addition to overexpressing *TNFAIP3*, the cells were also treated with 2.5 mM of 3-MA, an autophagy inhibitor. (A) OCI-LY3 cell viability measured by CCK-8 assay (n = 3). (B) Colony formation assay photographs depicting proliferation of OCI-LY3 cells and the quantification of colony numbers in each group (n = 3). (C) Levels of OCI-LY3 cell apoptosis as measured in flow cytometry assay (n = 3). (D) Transwell assay photographs and the quantification of migrating OCI-LY3 cells (n = 3). Scale bar: 50 µm. (E) Analysis of LC3 expression in OCI-LY3 cells by means of fluorescent staining assay (n = 3). Scale bar: 25 µm. (F) Western blotting detection of LC3I, LC3II and p62, and the quantification of p62 protein level and LC3II/LC3I ratio in transfected OCI-LY3 cells treated with 3-MA (n = 3). $^{**}p < 0.01$.

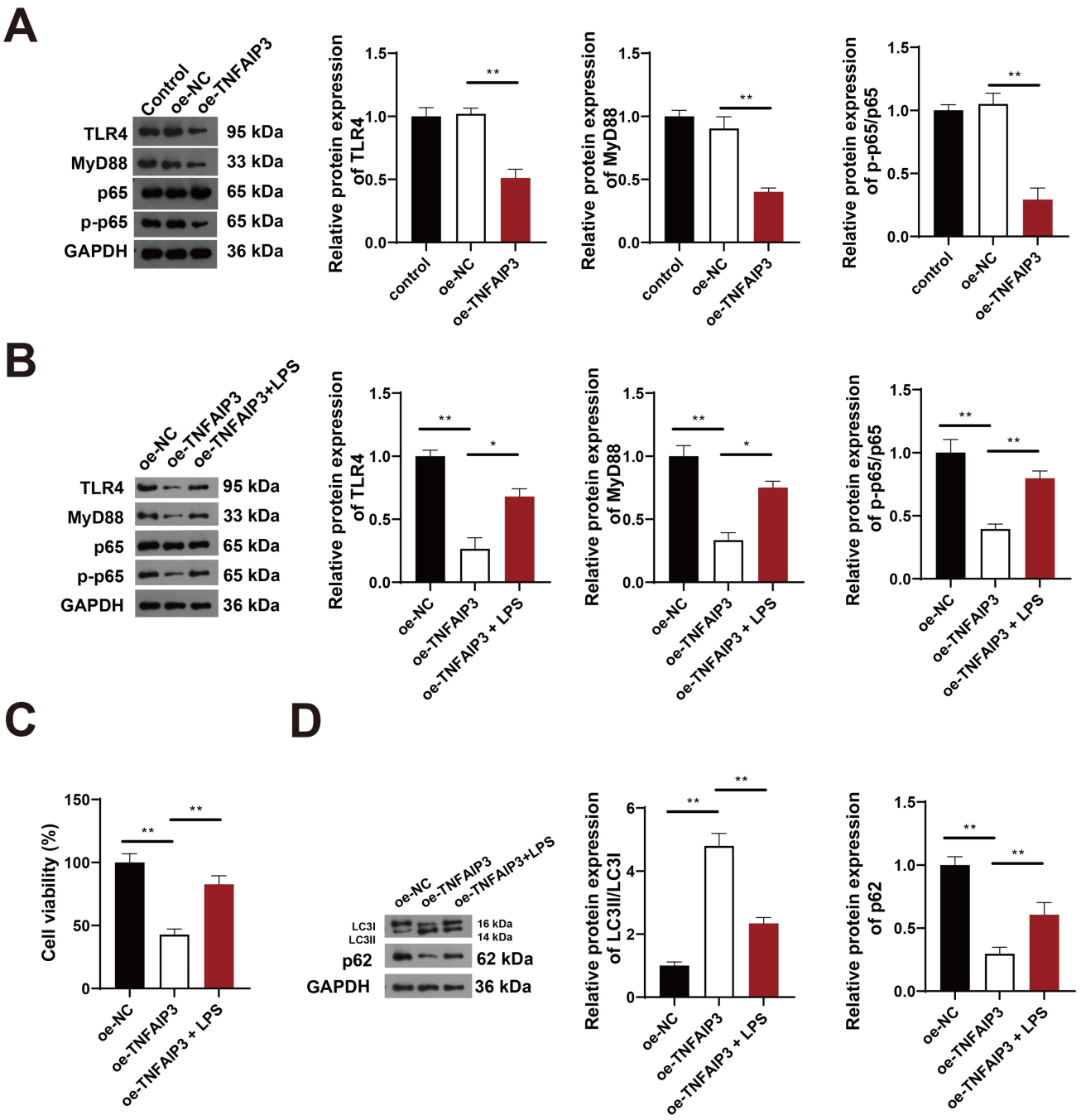

Fig. 5. *TNFAIP3* overexpression induced autophagy in human DLBCL cells through toll-like receptor 4 (TLR4)/MyD88/nuclear factor kappa B (NF-κB) signaling pathway. (A) Western blotting detection of TLR4, MyD88, and phosphorylated-Transcription Factor NF-Kappa-B P65 Subunit (p-p65)/p65, and the quantification of their protein levels in OCI-LY3 cells (n = 3). In addition to *TNFAIP3* overexpression, administration of 20 ng/mL lipopolysaccharide (LPS), an agonist of TLR4, was performed as a pre-treatment to the OCI-LY3 cells. (B) Western blotting detection of TLR4, MyD88, and p-p65/p65, and the quantification of their protein levels in OCI-LY3 cells pre-treated with LPS (n = 3). (C) OCI-LY3 cell viability as measured by CCK-8 assay (n = 3). (D) Western blotting detection of p62, LC3I and LC3II, and the quantification of p62 protein level and LC3II/LC3I ratio in OCI-LY3 cells pre-treated with LPS (n = 3). $^{*}p < 0.05$, $^{**}p < 0.01$.

tial therapeutic targets and markers for improving DLBCL prognosis [37]. The current study showed downregulated *TNFAIP3* expression in DLBCL. Besides, the cell transfection experiment of this study confirmed that the overexpression of *TNFAIP3* resulted in suppressed proliferation and migration of human DLBCL cells, as well as heightened cell apoptosis. These findings suggest that *TNFAIP3* acts as a tumor suppressor in DLBCL.

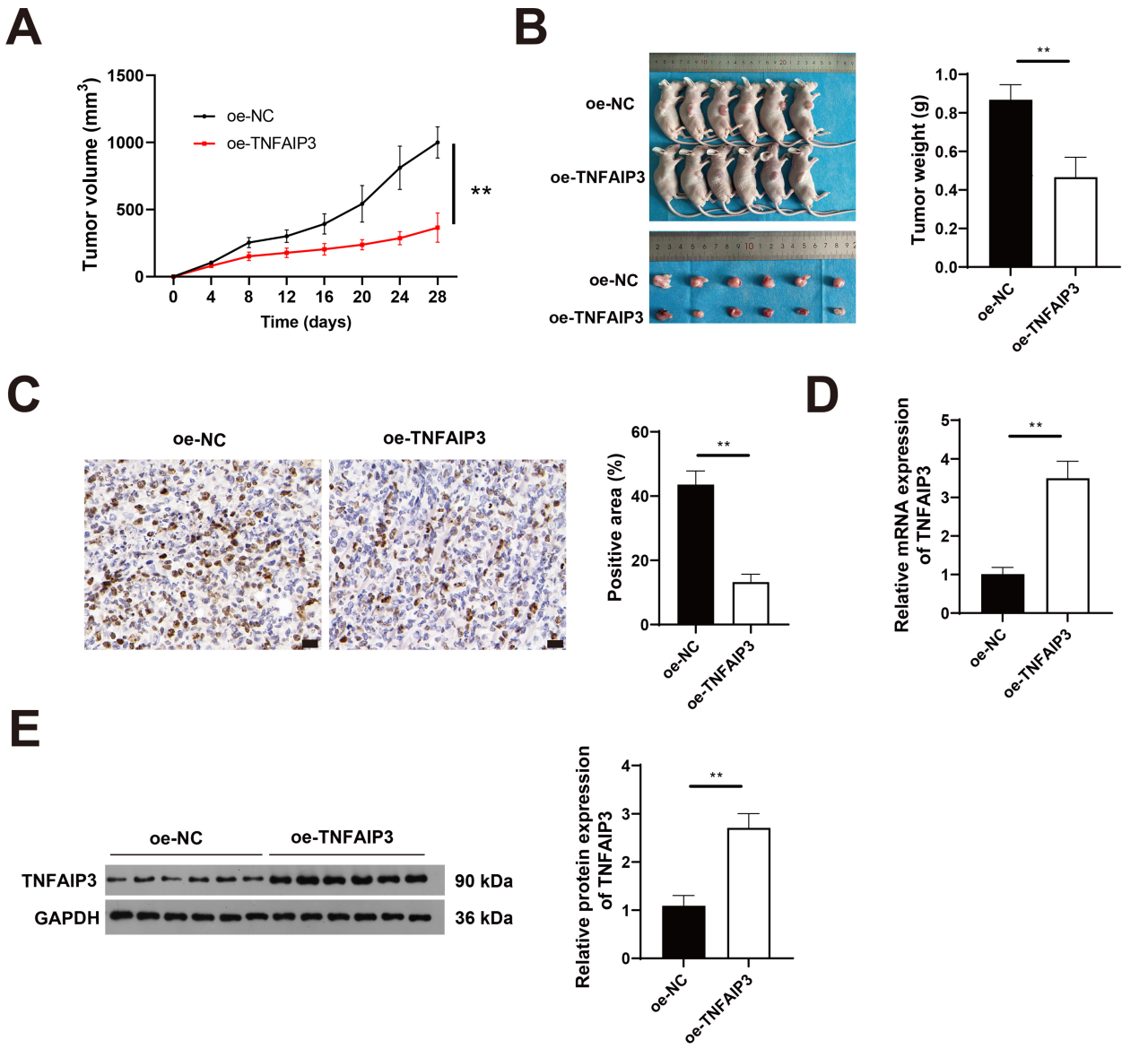

Fig. 6. *TNFAIP3* overexpression suppressed DLBCL tumor growth *in vivo*. (A,B) Tumor volume changes over 28 days in mice bearing DLBCL tumors (n = 6); photographs of experimental mice and resected tumors, as well as the comparison of tumor weight (n = 6). (C) Immunohistochemical detection of Ki67 expression in tumor tissues (n = 6). Scale bar: 20 µm. (D) *TNFAIP3* mRNA expression in tumor tissue (n = 6). (E) Western blotting detection of TNFAIP3 protein and the quantification of its expression in tumor tissues (n = 6). $^{**}p < 0.01$.

Aberrant expression of *TNFAIP3* has been detected in various tumors, correlating with tumor development and prognosis. TNFAIP3 is a potential regulator of Fibroblast Growth Factor Receptor 1- Mitogen-Activated Protein Kinase Kinase-Mitogen-Activated Protein Kinase (FGFR1-MEK-ERK)-promoted stem cells in Aldehyde Dehydrogenases (ALDH)-positive breast cancer [37]. Despite being scarcely expressed in colorectal cancer (CRC), TNFAIP3 plays a prominent role in inhibiting CRC cell proliferation [38]. In addition, silencing of *TNFAIP3* promotes the invasion and proliferation of lung cancer cells [39]. However, the depletion of *TNFAIP3* attenuates the proliferation capacity of gastric cancer cells [40]. Of note, *circ0008399*/WTAP/TNFAIP3 activation reduced the chemosensitivity of bladder cancer to Cisplatin [41]. Further, a previous study showed that *TNFAIP3* expression was downregulated in DLBCL patients, and *TNFAIP3* overexpression in DLBCL cells strengthened the suppressive effect of rituximab [42]. Consistent with these prior findings, our study confirmed that overexpression of *TNFAIP3* can promote apoptosis of DLBCL cells and attenuate their viability and migration. The mechanism underlying the *TNFAIP3*-mediated inhibition of DLBCL cellular activity was further explored in this study.

Autophagy is a complex process that maintains metabolic homeostasis through the formation of autophagic

vesicles and autophagic lysosomes that remove damaged cellular proteins and organelles [43]. Autophagy also plays an important role in tumors by inducing apoptosis and thus inhibiting tumor progression. LC3 protein is the key protein implicated in the generation of phagocytic vesicles in the endoplasmic reticulum and the cytoplasmic membrane during autophagy. There are two forms of LC3, namely LC3I and LC3II [44,45]. *TNFAIP3* promotes CD4 T cell survival by limiting mTOR and triggering autophagy [46]. In addition, *TNFAIP3* inhibits mTOR signaling and promotes autophagy to reduce the degeneration of inflammatory human nucleus pulposus cells [20]. In this study, to investigate the role of *TNFAIP3*-mediated autophagy on DLBCL cell viability, we treated the OCI-LY3 cells with 3-MA, which is an autophagy inhibitor. Our findings showed that 3-MA intervention could reverse the suppressive effect of *TNFAIP3* overexpression on DLBCL cell viability, indicating that TNFAIP3 attenuates DLBCL cell viability by inducing autophagy.

It has been reported that the TLR4-mediated signaling pathway induces DLBCL development [47,48], and inhibits tumor cell apoptosis in lung cancer [49], ovarian cancer [50], and myeloma [51]. MyD88 induction by diethylnitrosamine has also been shown to promote DLBCL development [52]. Besides, TNFAIP3 diminished Oxygen glucose deprivation/re-oxygenation (OGD/R)-induced neuronal damage by controlling TLR4/MyD88/NF-κB signaling [53]. In this study, *TNFAIP3* intervention dramatically downregulated TLR4, MyD88, and p-p65/p65 levels. To confirm whether TNFAIP3 induces autophagy via the TLR4/MyD88/NF-κB signaling axis, OCI-LY3 cells were pre-treated with 20 ng/mL LPS (TLR4 agonist), which reversed the suppressive effect of TNFAIP3 on OCI-LY3 cell viability. Meanwhile, LPS intervention also markedly negated the p62 downregulation and LC3II/LC3I ratio increase caused by *TNFAIP3* overexpression, indicating that *TNFAIP3* can inhibit DLBCL progression by inducing autophagy via suppression of TLR4/MyD88/NF-κB axis. Further, we confirmed that TNFAIP3 expression was downregulated *in vivo*, and TNFAIP3 might play an anti-tumor role by inhibiting the growth of tumors.

Several limitations of this study should be acknowledged. Firstly, the mechanism of TNFAIP3-induced autophagy in DLBCL was not deeply investigated using *in vivo* models in this study. Secondly, the present study did not delve into exploring the molecules acting downstream of the TNFAIP3-induced autophagy pathway.

Conclusion

This study presents a novel mechanism underlying TNFAIP3-mediated inhibition of DLBCL progression by inducing autophagy through inhibiting TLR4/MyD88/NF-κB axis, weaving a new tapestry to aid the development of innovative targeted molecular therapy for DLBCL. Future experiments will focus on exploring the role of TNFAIP3 in epithelial-mesenchymal transition and angiogenesis in the setting of DLBCL cells. Despite the affirmative findings stemming from this study, any DLBCL treatments aimed at upregulating the expression of TNFAIP3 need to be further validated in clinical trials to verify the protective role of TNFAIP3 in tumors.

Availability of Data and Materials

The datasets used and/or analyzed during the current study are available from the corresponding author upon reasonable request.

Author Contributions

FYN: conceptualization, writing–original draft, funding acquisition and formal analysis. HFW: data curation, resources, project administration, validation. ZYL: data curation, validation, supervision, visualization. JPL: conceptualization and writing–review & editing, validation. All authors contributed significantly to editorial changes of important content. All authors have participated sufficiently in the work and agreed to be accountable for all aspects of the work. All authors read and approved the final manuscript.

Ethics Approval and Consent to Participate

This study was approved by the Institutional Animal Care and Use Committee of Yangzhou University (No: 202305011).

Acknowledgment

Not applicable.

Funding

This work was supported by [Zhejiang Medical and Health Science and Technology Project] [numbers 2022KY541, 2024KY772].

Conflict of Interest

The authors declare no conflict of interest.

References

[1] He MY, Kridel R. Treatment resistance in diffuse large B-cell lymphoma. Leukemia. 2021; 35: 2151–2165.

[2] Liang XJ, Song XY, Wu JL, Liu D, Lin BY, Zhou HS, *et al*. Advances in Multi-Omics Study of Prognostic Biomarkers of Diffuse Large B-Cell Lymphoma. International Journal of Biological Sciences. 2022; 18: 1313–1327.

[3] Iacoboni G, Zucca E, Ghielmini M, Stathis A. Methodology of clinical trials evaluating the incorporation of new drugs in the first-line treatment of patients with diffuse large B-cell lym-

phoma (DLBCL): a critical review. Annals of Oncology. 2018; 29: 1120–1129.

[4] Kuang Z, Li X, Liu R, Chen S, Tu J. Comprehensive Characterization of Cachexia-Inducing Factors in Diffuse Large B-Cell Lymphoma Reveals a Molecular Subtype and a Prognosis-Related Signature. Frontiers in Cell and Developmental Biology. 2021; 9: 648856.

[5] Ollila TA, Olszewski AJ. Extranodal Diffuse Large B Cell Lymphoma: Molecular Features, Prognosis, and Risk of Central Nervous System Recurrence. Current Treatment Options in Oncology. 2018; 19: 38.

[6] Momtazi G, Lambrecht BN, Naranjo JR, Schock BC. Regulators of A20 (TNFAIP3): new drug-able targets in inflammation. American Journal of Physiology. Lung Cellular and Molecular Physiology. 2019; 316: L456–L469.

[7] Wang Y, Song M, Zhou P, Wang J, Zheng J, Xu H. TNFAIP3-upregulated RIP3 exacerbates acute pancreatitis via activating NLRP3 inflammasome. International Immunopharmacology. 2021; 100: 108067.

[8] Jallades L, Baseggio L, Sujobert P, Huet S, Chabane K, Callet-Bauchu E, *et al*. Exome sequencing identifies recurrent *BCOR* alterations and the absence of *KLF2*, *TNFAIP3* and *MYD88* mutations in splenic diffuse red pulp small B-cell lymphoma. Haematologica. 2017; 102: 1758–1766.

[9] Liu K, Yao H, Wen Y, Zhao H, Zhou N, Lei S, *et al*. Functional role of a long non-coding RNA LIFR-AS1/miR-29a/TNFAIP3 axis in colorectal cancer resistance to pohotodynamic therapy. Biochimica et Biophysica Acta. Molecular Basis of Disease. 2018; 1864: 2871–2880.

[10] Feng Y, Zhang Y, Cai Y, Liu R, Lu M, Li T, *et al*. A20 targets PFKL and glycolysis to inhibit the progression of hepatocellular carcinoma. Cell Death & Disease. 2020; 11: 89.

[11] Sharif-Askari FS, Al-Khayyal N, Talaat I, Sharif-Askari NS, Rawat S, Jundi M, *et al*. Immunohistochemical Assessment of TNFAIP3/A20 Expression Correlates With Early Tumorigenesis in Breast Cancer. Anticancer Research. 2021; 41: 739–745.

[12] Wisnieski F, Santos LC, Calcagno DQ, Geraldis JC, Gigek CO, Anauate AC, *et al*. The impact of DNA demethylation on the upregulation of the NRN1 and TNFAIP3 genes associated with advanced gastric cancer. Journal of Molecular Medicine. 2020; 98: 707–717.

[13] Wang M, Li S. Bladder polypoid cystitis-derived A20 associates with tumorigenesis. Cell Biochemistry and Biophysics. 2013; 67: 669–673.

[14] Levine B, Kroemer G. Biological Functions of Autophagy Genes: A Disease Perspective. Cell. 2019; 176: 11–42.

[15] Wu M, Zhang P. EGFR-mediated autophagy in tumourigenesis and therapeutic resistance. Cancer Letters. 2020; 469: 207–216.

[16] Manent J, Banerjee S, de Matos Simoes R, Zoranovic T, Mitsiades C, Penninger JM, *et al*. Autophagy suppresses Ras-driven epithelial tumourigenesis by limiting the accumulation of reactive oxygen species. Oncogene. 2017; 36: 5576–5592.

[17] Cui Y, Xu H, Yang Y, Zhao D, Wen Y, Lv C, *et al*. The regulation of miR-320a/XBP1 axis through LINC00963 for endoplasmic reticulum stress and autophagy in diffuse large B-cell lymphoma. Cancer Cell International. 2021; 21: 305.

[18] Serramito-Gómez I, Boada-Romero E, Slowicka K, Vereecke L, Van Loo G, Pimentel-Muiños FX. The anti-inflammatory protein TNFAIP3/A20 binds the WD40 domain of ATG16L1 to control the autophagic response, NFKB/NF-κB activation and intestinal homeostasis. Autophagy. 2019; 15: 1657–1659.

[19] Yan K, Wu C, Ye Y, Li L, Wang X, He W, *et al*. A20 inhibits osteoclastogenesis via TRAF6-dependent autophagy in human periodontal ligament cells under hypoxia. Cell Proliferation. 2020; 53: e12778.

[20] Chen J, Ma Y, Yang Z, Lan H, Liu G, Zhang Y, *et al*. TNFAIP3 ameliorates the degeneration of inflammatory human nucleus pulposus cells by inhibiting mTOR signaling and promoting autophagy. Aging. 2020; 12: 24242–24254.

[21] Ma C, Wei X, Wang F, Zhang T, Jiang Y, Meng Z, *et al*. Tumor necrosis factor α-induced protein 3 mediates inflammation and neuronal autophagy in Parkinson's disease via the NFκB and mTOR pathways. Neuroscience Letters. 2023; 805: 137223.

[22] Paul S, Bhardwaj M, Kang SC. GSTO1 confers drug resistance in HCT 116 colon cancer cells through an interaction with TNFαIP3/A20. International Journal of Oncology. 2022; 61: 136.

[23] Nouri Y, Weinkove R, Perret R. T-cell intrinsic Toll-like receptor signaling: implications for cancer immunotherapy and CAR T-cells. Journal for Immunotherapy of Cancer. 2021; 9: e003065.

[24] Guo J, Liao M, Wang J. TLR4 signaling in the development of colitis-associated cancer and its possible interplay with microRNA-155. Cell Communication and Signaling. 2021; 19: 90.

[25] Afroz R, Tanvir EM, Tania M, Fu J, Kamal MA, Khan MA. LPS/TLR4 Pathways in Breast Cancer: Insights into Cell Signalling. Current Medicinal Chemistry. 2022; 29: 2274–2289.

[26] Chen CY, Kao CL, Liu CM. The Cancer Prevention, Anti-Inflammatory and Anti-Oxidation of Bioactive Phytochemicals Targeting the TLR4 Signaling Pathway. International Journal of Molecular Sciences. 2018; 19: 2729.

[27] Burgueño JF, Fritsch J, González EE, Landau KS, Santander AM, Fernández I, *et al*. Epithelial TLR4 Signaling Activates DUOX2 to Induce Microbiota-Driven Tumorigenesis. Gastroenterology. 2021; 160: 797–808.e6.

[28] Shetab Boushehri MA, Lamprecht A. TLR4-Based Immunotherapeutics in Cancer: A Review of the Achievements and Shortcomings. Molecular Pharmaceutics. 2018; 15: 4777–4800.

[29] Jia Y, Yin C, Ke W, Liu J, Guo B, Wang X, *et al*. Alpha-ketoglutarate alleviates cadmium-induced inflammation by inhibiting the HIF1A-TNFAIP3 pathway in hepatocytes. The Science of the Total Environment. 2023; 878: 163069.

[30] Sun JR, Zhang X, Zhang Y. MiR-214 prevents the progression of diffuse large B-cell lymphoma by targeting PD-L1. Cellular & Molecular Biology Letters. 2019; 24: 68.

[31] Zhao Z, Xue J, Zhao X, Lu J, Liu P. Prognostic role of autophagy-related proteins in epithelial ovarian cancer: a meta-analysis of observational studies. Minerva Medica. 2017; 108: 277–286.

[32] Mareninova OA, Jia W, Gretler SR, Holthaus CL, Thomas DDH, Pimienta M, *et al*. Transgenic expression of GFP-LC3 perturbs autophagy in exocrine pancreas and acute pancreatitis responses in mice. Autophagy. 2020; 16: 2084–2097.

[33] Zhang H, Zhang Y, Zhu X, Chen C, Zhang C, Xia Y, *et al*. DEAD Box Protein 5 Inhibits Liver Tumorigenesis by Stimulating Autophagy via Interaction with p62/SQSTM1. Hepatology. 2019; 69: 1046–1063.

[34] Haghdoost-Yazdi H, Abbaszadeh HA, Hamidabadi HG, Darabi S, Darabi L, Rajaei F, *et al*. Trehalose and carnosic acid induced LC3I, LC3II ratio, P62 down-regulation and cleaved caspase 3 expression in neural stem cells. Bratislavske Lekarske Listy. 2022; 123: 901–907.

[35] Harrington F, Greenslade M, Talaulikar D, Corboy G. Genomic characterisation of diffuse large B-cell lymphoma. Pathology. 2021; 53: 367–376.

[36] Pi M, Kuang H, Yue C, Yang Q, Wu A, Li Y, *et al*. Targeting metabolism to overcome cancer drug resistance: A promising therapeutic strategy for diffuse large B cell lymphoma. Drug Resistance Updates: Reviews and Commentaries in Antimicrobial and Anticancer Chemotherapy. 2022; 61: 100822.

[37] Feng W, Gao M, Yang M, Li X, Gan Z, Wu T, *et al*. TNFAIP3

promotes ALDH-positive breast cancer stem cells through FGFR1/MEK/ERK pathway. Medical Oncology. 2022; 39: 230.

[38] Li J, Ren S, Zhang Y, Wu B, He M, Shan Z, *et al*. Clinical and Basic Evaluation of the Effects of Upregulated TNFAIP3 Expression on Colorectal Cancer. Disease Markers. 2022; 2022: 1263530.

[39] Liao Y, Cao L, Wang F, Pang R. miR-605-5p promotes invasion and proliferation by targeting TNFAIP3 in non-small-cell lung cancer. Journal of Cellular Biochemistry. 2020; 121: 779–787.

[40] Du B, Liu M, Li C, Geng X, Zhang X, Ning D, *et al*. The potential role of TNFAIP3 in malignant transformation of gastric carcinoma. Pathology, Research and Practice. 2019; 215: 152471.

[41] Wei W, Sun J, Zhang H, Xiao X, Huang C, Wang L, *et al*. *Circ0008399* Interaction with WTAP Promotes Assembly and Activity of the m^6A Methyltransferase Complex and Promotes Cisplatin Resistance in Bladder Cancer. Cancer Research. 2021; 81: 6142–6156.

[42] Zhang L, Zhou S, Zhou T, Li X, Tang J. Potential of the tumor derived extracellular vesicles carrying the miR 125b 5p target TNFAIP3 in reducing the sensitivity of diffuse large B cell lymphoma to rituximab. International Journal of Oncology. 2021; 58: 31.

[43] Koustas E, Sarantis P, Theoharis S, Saetta AA, Chatziandreou I, Kyriakopoulou G, *et al*. Autophagy-related Proteins as a Prognostic Factor of Patients With Colorectal Cancer. American Journal of Clinical Oncology. 2019; 42: 767–776.

[44] Zhou J, Jiang YY, Chen H, Wu YC, Zhang L. Tanshinone I attenuates the malignant biological properties of ovarian cancer by inducing apoptosis and autophagy via the inactivation of PI3K/AKT/mTOR pathway. Cell Proliferation. 2020; 53: e12739.

[45] Li D, Yan M, Sun F, Song J, Hu X, Yu S, *et al*. miR-498 inhibits autophagy and M2-like polarization of tumor-associated macrophages in esophageal cancer via MDM2/ATF3. Epigenomics. 2021; 13: 1013–1030.

[46] Matsuzawa Y, Oshima S, Takahara M, Maeyashiki C, Nemoto Y, Kobayashi M, *et al*. TNFAIP3 promotes survival of CD4 T cells by restricting MTOR and promoting autophagy. Autophagy. 2015; 11: 1052–1062.

[47] Akhter A, Masir N, Elyamany G, Phang KC, Mahe E, Al-Zahrani AM, *et al*. Differential expression of Toll-like receptor (TLR) and B cell receptor (BCR) signaling molecules in primary diffuse large B-cell lymphoma of the central nervous system. Journal of Neuro-Oncology. 2015; 121: 289–296.

[48] Wang X, Li X, Zhang X, Zang L, Yang H, Zhao W, *et al*. Toll-like receptor 4-induced inflammatory responses contribute to the tumor-associated macrophages formation and infiltration in patients with diffuse large B-cell lymphoma. Annals of Diagnostic Pathology. 2015; 19: 232–238.

[49] Yuan R, Zhao W, Wang QQ, He J, Han S, Gao H, *et al*. Cucurbitacin B inhibits non-small cell lung cancer in vivo and in vitro by triggering TLR4/NLRP3/GSDMD-dependent pyroptosis. Pharmacological Research. 2021; 170: 105748.

[50] Xu R, Ruan Y, Zhang L, Gu Y, Liu M. Fraxetin suppresses the proliferation, migration, and invasion of ovarian cancer cells by inhibiting the TLR4/STAT3 signaling pathway. Immunopharmacology and Immunotoxicology. 2023; 45: 287–294.

[51] Giallongo C, Tibullo D, Puglisi F, Barbato A, Vicario N, Cambria D, *et al*. Inhibition of TLR4 Signaling Affects Mitochondrial Fitness and Overcomes Bortezomib Resistance in Myeloma Plasma Cells. Cancers. 2020; 12: 1999.

[52] Visco C, Tanasi I, Quaglia FM, Ferrarini I, Fraenza C, Krampera M. Oncogenic Mutations of MYD88 and CD79B in Diffuse Large B-Cell Lymphoma and Implications for Clinical Practice. Cancers. 2020; 12: 2913.

[53] Yan Z, Chen Y, Zhang X, Hua L, Huang L. Neuroprotective Function of TNFAIP3 Interacting Protein 2 Against Oxygen and Glucose Deprivation/Reoxygenation-Induced Injury in Hippocampal Neuronal HT22 Cells Through Regulation of the TLR4/MyD88/NF-κB Pathway. Neuropsychiatric Disease and Treatment. 2021; 17: 2219–2227.